PAPER

Check for updates

Conformational flexibility of the disaccharide β-L-Fuc*p*-(1→4)-α-D-Glc*p*-OMe as deduced from NMR spectroscopy experiments and computer simulations

Wojciech Plazinski, [ID] [a,b] Thibault Angles d'Ortoli [ID] [c] and Göran Widmalm [ID] *[c]

Carbohydrates in biological systems are referred to as glycans and modification of their structures is a hallmark indicator of disease. Analysis of the three-dimensional structure forms the basis for further insight into how they function and comparison of crystal structure with solution-state conformation(s) is particularly relevant, which has been performed for the disaccharide β-L-Fuc*p*-(1→4)-α-D-Glc*p*-OMe. In water solution the conformational space at the glycosidic linkage between the two sugar residues is identified from molecular dynamics (MD) simulations as having a low-energy *exo-syn* conformation, deviating somewhat from the solid-state conformation, and two *anti*-conformational states, *i.e.*, *anti*-ϕ and *anti*-ψ, indicating flexibility at the glycosidic linkage. NMR data were obtained from 1D ^{1}H,^{1}H-NOESY and STEP-NOESY experiments, measurement of transglycosidic $^3J_{CH}$ coupling constants and NMR spin-simulation. The free energy profile of the ω torsion angle computed from MD simulation was in excellent agreement with the rotamer distribution from NMR experiment being for *gt:gg:tg* 38 : 53 : 9, respectively, with a proposed inter-residue O5′···HO6 hydrogen bond being predominant in the *gg* rotamer. Quantum mechanics methodology was used to calculate transglycosidic NMR $^3J_{CH}$ coupling constants, averaged over a conformational ensemble of structures representing various rotamers of exocyclic groups, in good to excellent agreement with Karplus-type relationships previously developed. Furthermore, ^{1}H and ^{13}C NMR chemical shifts were calculated using the same methodology and were found to be in excellent agreement with experimental data.

Introduction

Glycans, carbohydrates in biological systems, are often linked to proteins or lipids as glycoconjugates, although some are not, such as hyaluronic acid, and the glycome is described as all of the glycans in a particular cell, tissue or organism. These glycans are important in relation to infection and immunity where regulatory effects depend on mediated interactions with glycan binding proteins that have carbohydrate binding domains.[1] Thus, a thorough understanding of recognition mechanisms facilitates the development of glycan-mimetic anti-infective and anti-inflammatory drugs. Malfunction of glycan regulation plays a central role in disease processes as glycans, for example, control protein stability, receptor dimerization, and binding to carbohydrate-specific receptors such as

selectins that mediate immune cell adhesion.[2] Changes in glycan structure on glycoproteins are associated with cancer, *e.g.*, in the form of novel glycan-based epitopes, which are markers of oncogenic transformation, or by accumulation of 5-*N*-glycolylneuraminic acid (a sialic acid form not synthesized by humans) in cancerous tissues. Moreover, in autoimmune disease changes are evident due to loss of galactose residues and exposure of terminal *N*-acetylglucosamine residues on *N*-glycans of IgG antibodies.[3] Identifying the three-dimensional (3D) structure of glycans and how alteration of these will affect pathological conditions, biomarkers and therapeutic targets are of prime importance to cure disease.[4]

Detailed information about the 3D structure of an oligosaccharide may be obtained from its crystal structure, though crystallization of highly hydrophilic carbohydrate molecules can be difficult and elusive. However, when it is available, a comparison of its solid-state conformation[5] can be made with that or those identified by NMR experiments[6] in conjunction with molecular dynamics (MD) simulations.[7] In the crystal structure of β-L-Fuc*p*-(1→4)-α-D-Glc*p*-OMe (F4G)[8] the glycosidic torsion angles $\phi = -6°$ and $\psi = +34°$ between the two sugar

[a] Jerzy Haber Institute of Catalysis and Surface Chemistry, Polish Academy of Sciences, 30-239 Krakow, Poland
[b] Department of Biopharmacy, Medical University of Lublin, 20-093 Lublin, Poland
[c] Department of Organic Chemistry, Arrhenius Laboratory, Stockholm University, S-106 91 Stockholm, Sweden. E-mail: goran.widmalm@su.se
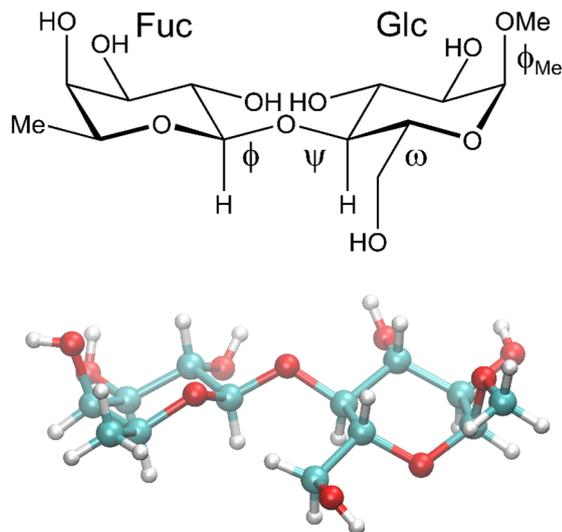
This journal is © The Royal Society of Chemistry 2023

Org. Biomol. Chem., 2023, **21**, 6979–6994 | **6979**

Fig. 1 Schematic (top) and crystal structure[8] (bottom) of β-L-Fuc*p*-(1→4)-α-D-Glc*p*-OMe. The ω torsion angle is drawn in the *gauche–gauche* conformation in the schematic structure and has the *gauche–trans* conformation in the crystal structure.

residues, the former of which deviates a good deal from the *exo*-anomeric conformation[9] that would have $\phi \approx -50°$ (β-L-hexopyranoside), or as observed for the torsion angle to the *O*-methyl group having $\phi_{Me} = -56°$ (α-D-hexopyranoside), whereas the latter ψ torsion is tilted away from an eclipsed conformation (Fig. 1). The torsion angle of the *exo*-cyclic hydroxymethyl group of the glucose residue has the *gauche–trans* conformation with $\omega = 68°$, *i.e.*, slightly shifted from the staggered conformation.[10] To investigate conformational dynamics at the glycosidic linkage in general, to analyze solution-state conformation(s) in comparison to the conformation in the crystal and to unravel the importance of atomic interactions between the two sugar residues as well as to solvent molecules we have performed NMR experiments and computationally carried out MD simulations and quantum mechanical (QM) calculations on F4G.

Materials and methods

General

The synthesis and ^{1}H and ^{13}C NMR chemical shift assignments of the disaccharide β-L-Fuc*p*-(1→4)-α-D-Glc*p*-OMe were previously reported by Backman *et al.*[11] Atoms in the terminal fucosyl residue are denoted by a prime and those in the glucosyl residue are unprimed. The glycosidic torsion angles are defined as follows: ϕ = H1′–C1′–O4–C4, ψ = C1′–O4–C4–H4, ϕ_{Me} = H1–C1–O–C$_{Me}$; the torsion angle of the hydroxymethyl group is defined by ω = O5–C5–C6–O6.

NMR spectroscopy

The disaccharide sample was prepared in a 5 mm NMR tube in D$_2$O, pD ≈ 6, with a sample concentration of 50 mM. ^{1}H

NMR chemical shifts were referenced to internal sodium 3-trimethylsilyl-(2,2,3,3-^{2}H$_4$)-propanoate (TSP, δ_H 0.00). NMR experiments were carried out using a 600 MHz Bruker AVANCE III spectrometer equipped with a 5 mm inverse *Z*-gradient TXI (^{1}H/^{13}C/^{31}P) or with a 5 mm BBO probe, a 500 MHz Bruker AVANCE or a 700 MHz Bruker AVANCE III spectrometer, both of which were equipped with a 5 mm TCI *Z*-gradient cryoprobe. The temperature was calibrated by a methanol-d_4 sample,[12] and processing of the acquired data was carried out using TopSpin 3.1 (Bruker).

1D ^{1}H NMR spectra were recorded at 306 K with the 500, 600 and 700 MHz Bruker spectrometers. Chemical shifts and coupling constants were refined iteratively from ^{1}H NMR spectra with both the integral transform fitting mode and the total-lineshape mode of the PERCH NMR iterator PERCHit.[13,14] Starting values for the iteration were extracted from the experimental 1D spectra and the linewidths and lineshapes were part of the iterative refinement process of the spectral parameters.

The proton–proton cross-relaxation rates were determined at 600 MHz and 318 K employing both 1D ^{1}H,^{1}H-NOESY[15] and 1D ^{1}H,^{1}H-STEP-NOESY experiments.[16,17] In all cases, selective excitation was achieved by single PFGSE modules utilizing 50 ms r-SNOB shaped pulses for both the NOESY experiment and the STEP-NOESY experiment. The strengths of the first and second gradient pairs were 15% and 40%, respectively, of the maximum (55.7 G cm^{-1}) for the NOESY experiments. For the STEP-NOESY, the strengths of the gradients were set to 10% or 6.5% for the first and 45% or 15% for the second excitation, respectively. During the STEP-NOESY experiment the resonance from H1 was selectively excited and magnetization transferred to H3 using a 3.8 kHz DIPSI-2 spin-lock with a duration of 50 ms prior to selective excitation of H3. In the STEP-NOESY experiments, zero-quantum coherences were suppressed using the scheme devised by Thrippleton and Keeler,[18] where a 30–50 ms adiabatic Chirp pulse with a bandwidth of 20 kHz was applied together with a gradient pulse with 3% of the maximum power. In the NOESY experiment a 20 ms adiabatic Chirp pulse with a bandwidth of 40 kHz was used in combination with a gradient pulse at 3% of the maximum power. In the NOESY as well as the STEP-NOESY experiments, 9 cross-relaxation delays between 70 and 450 ms were collected for each of the excited spins. A spectral width of 6 ppm was sampled using 16k data points and 2048 transients were averaged. The repetition time was 8–10 s, *i.e.*, in all cases longer than 5 × T_1. Prior to Fourier transformation, the FIDs of the 1D experiments were zero-filled to 262k points and multiplied by an exponential line-broadening function of 2 Hz. Baseline correction was performed prior to integration, which used the same integration limits for all experiments within a series. The areas of relevant peaks were divided by the area of the inverted peak and analyzed as devised by Dixon *et al.*, *i.e.*, $I_j(\tau_{mix})/[\tau_{mix}I_j] = -\sigma_{ij}$, where I_j is the intensity of the signal at nucleus j following selective excitation of nucleus i with intensity I_i in the 1D ^{1}H,^{1}H-NOESY experiments.[19] By extrapolation of the individual σ_{ij} data, the proton–proton cross-relaxation

6980 | *Org. Biomol. Chem.*, 2023, **21**, 6979–6994

This journal is © The Royal Society of Chemistry 2023

rates were obtained from the intercept with the ordinate axis at $\tau_{\text{mix}} = 0$.

Measurements of the transglycosidic carbon–proton coupling constants were performed at 600 MHz and 300 K using J-HMBC experiments[20] and one-dimensional long-range experiments essentially as devised by Nishida et al.[21,22] For the J-HMBC experiments, a threefold low-pass J-filter (J = 140 Hz, 155 Hz and 175 Hz) was used to suppress $^1J_{\text{CH}}$. A scaling factor of 51.5, which was calculated from $\kappa = \Delta/t_1^{\max}$, where Δ was at least 60% of the inverse of the smallest coupling constant to be measured, was used to scale the coupling in the indirect (F_1) dimension. Spectral widths of 6 ppm for ^{1}H and 140 ppm for ^{13}C were used. The experiments were performed with 16 384 × 512 points and 16 scans per t_1 increment with the echo/antiecho method. Forward linear prediction to 1024 points in the F_1 dimension and subsequent zero-filling to 8192 points was applied prior to Fourier transformation. Coupling constants were extracted from 1D projections of the resonances of interest. One-dimensional long-range (1DLR) experiments employed ^{13}C site-selective excitation with a Gaussian shaped pulse of 80 ms duration. The delay used for suppression of $^1J_{\text{CH}}$ was set to (145 Hz)$^{-1}$ and the time of the delay between excitation and coherence transfer, for evolution of the long-range coupling, was set by using nominal values of 8–16 Hz; an acquisition time of 3 s, 10 240–13 312 transients and 50k data points were used. Zero-filling was performed to 512k data points and an exponential line-broadening function lb = 0.6 Hz was applied prior to Fourier transformation. Subsequently, the $^3J_{\text{CH}}$ coupling constants were extracted by the J doubling methodology[23] implemented in-house by a MATLAB script.

Conformational analysis from experimental NMR data

From the MD simulations (vide infra) of F4G, three-bond spin–spin NMR coupling constants were calculated according to the following equations:

$$^3J_{\text{H1',C4}}(\phi) = 6.54 \cos^2(\phi - \Delta) - 0.62 \cos(\phi - \Delta) - 0.17 \quad (1)$$

$$^3J_{\text{C1',H4}}(\psi) = 6.54 \cos^2(\psi) - 0.62 \cos(\psi) + 0.33 \\ + 0.6 \exp(\kappa \cos(\phi_{\text{O5'}} - 180))/\exp(\kappa) \quad (2)$$

$$^3J_{\text{H5,H6}R} = 5.08 + 0.47 \cos(\omega) + 0.90 \sin(\omega) \\ - 0.12 \cos(2\omega) + 4.86 \sin(2\omega) \quad (3)$$

$$^3J_{\text{H5,H6}S} = 4.92 - 1.29 \cos(\omega) + 0.05 \sin(\omega) \\ + 4.58 \cos(2\omega) + 0.07 \sin(2\omega) \quad (4)$$

Heteronuclear transglycosidic Karplus-type relationships were employed, where for the ϕ torsion angle the phase shift (Δ) was set to $-12°$ based on the anomeric and absolute configuration of the β-L-Fucp residue.[24] The variable in-plane effect affecting the coupling constant related to the ψ torsion angle was implemented by setting $\kappa = 8$.

^{1}H,^{1}H distances in F4G were obtained from NMR experiments by applying the isolated spin-pair approximation (ISPA) $r_{ij} = r_{\text{ref}}(\sigma_{\text{ref}}/\sigma_{ij})^{1/6}$, where the reference distance r_{ref} is an average over the MD trajectory and σ is the proton–proton cross-relaxation rate constant between directly interacting proton pairs. Effective proton–proton distances were calculated from the MD simulation (using water as explicit solvent) according to $r_{ij} = \langle r_{ij}^{-6} \rangle^{-1/6}$, where the brackets indicate averaging over all frames of the trajectory. The Karplus-type relationships for the conformational dependence of the ω torsion angle developed by Stenutz et al.[10] were used to determine the populations of the gt, gg and tg states from $^3J_{\text{H5,H6}R}$ and $^3J_{\text{H5,H6}S}$ coupling constants.

Computer simulations

The computations were carried out with a single molecule of F4G and involved: (i) MD simulations performed with a classical additive force field, (ii) MD simulations performed according to hybrid QM/MM methodology, and (iii) ab initio QM calculations. Additionally, the classical MD simulations were applied for the α-D-Glcp-OMe monosaccharide.

The classical MD simulations were carried out with the CHARMM force field[25,26] by using the GROMACS 2016.4 package.[27] The CHARMM parameters in the GROMACS-readable format were prepared by using the CHARMM-GUI online server (**https://www.charmm-gui.org**).[28] The considered MD system consisted of one F4G molecule solvated by ca. 1450 explicit water molecules within a cubic box simulated under periodic boundary conditions. The box edges (of initial dimensions corresponding to 3.5 × 3.5 × 3.5 nm^3) were preoptimized by a 1 ns constant–pressure MD equilibration at 1 bar and 298 K, ensuring an effective solvent density appropriate for the conditions in the subsequent production simulations. After equilibration, the unbiased MD simulation was carried out for 300 ns. The data (interaction energies and trajectory) were saved every 1 ps. During the MD simulation, the temperature was maintained close to its reference value (298 K) by applying the V-rescale thermostat,[29] whereas for constant pressure (1 bar, isotropic coordinate scaling) the Parrinello–Rahman barostat[30] was used with a relaxation time of 0.4 ps. The equations of motion were integrated with a time step of 2 fs using the leap-frog scheme.[31] The translational center-of-mass motion was removed every timestep separately for the solute and the solvent. The full rigidity of the TIP3P[32] water molecules was enforced by application of the SETTLE procedure,[33] whereas for the solute the hydrogen-containing bond lengths were constrained by application of the LINCS procedure with a relative geometric tolerance of 10^{-4}.[34] The electrostatic interactions were modeled by using the particle-mesh Ewald (PME) method[35] with the cutoff set to 1.2 nm, while van der Waals interactions (Lennard-Jones potentials) were switched off between 1.0 and 1.2 nm. The same simulation setup was applied also in the case of α-D-Glcp-OMe.

The analysis of the unbiased MD simulations of F4G included: (i) the occurrence of hydrogen bonding; (ii) the population of the hydroxymethyl group rotamers; (iii) the interatomic distances for selected atom pairs; (iv) the conformation of glycosidic linkages; and (v) the population of the individual conformers, distinguished on the basis of the

This journal is © The Royal Society of Chemistry 2023

Org. Biomol. Chem., 2023, **21**, 6979–6994 | **6981**

rotation of the exocyclic groups. In step (i), the default, GROMACS-inherent geometrical criteria were applied, *i.e.*, a cutoff angle (hydrogen–donor–acceptor) of 30° and a cutoff radius (X–acceptor) of 0.35 nm. In step (ii), the conformation of the O5–C5–C6–O6 torsion angle (ω) was assigned to one of the three possible staggered conformers, based on its value, *i.e.*, *gt* (staggered conformation at 60°), *gg* (−60°), and *tg* (180°). In step (iv), the ϕ and ψ glycosidic torsion angles were defined by the following quadruplets of atoms: ϕ = H1′–C1′–O4–C4 and ψ = C1′–O4–C4–H4. The purpose of step (v) was to optimize the *ab initio* calculations by taking into account a broad set of conformationally distinct structures. Each F4G structure present in the MD trajectory was analyzed with respect to the conformation of all rotatable bonds associated with exocyclic groups of the molecule. The conformation of each torsion angle was assigned to be one of the three possible staggered conformers, based on the smallest deviation from the optimal value. The results of such assignment were sorted and the 400 most frequently occurring individual rotamers were subjected to subsequent *ab initio* calculations.

The enhanced-sampling free energy calculations were focused on the 2D free energy maps associated with the glycosidic linkage conformation. The calculations relied on an enhanced sampling scheme combining[36] parallel tempering[37] and well-tempered metadynamics[38] as implemented in the PLUMED 2.3 plug-in.[39] The well-tempered metadynamics relied on Gaussian local functions of widths of 18°, an initial deposition rate of 0.01 kJ mol⁻¹ ps⁻¹ and a temperature parameter ΔT (defined according to eqn (2) of Barducci *et al.*[38]) of 1788 K. The parallel tempering relied on 16 metadynamics simulations carried out in parallel at different temperatures ranging from 298.0 to 363.2 K in steps of about 4.3 K, along with replica-exchange attempts performed at 2 ps intervals. The duration of metadynamics simulations was 10 ns. The remaining details of the simulation set-up were identical to those described earlier for the case of unbiased MD simulations. Additionally, the analogous enhanced-sampling calculations were carried out for F4G *in vacuo*. The simulation set-up was modified accordingly to account for the lack of solvent by turning off the pressure control and replacing the PME treatment of long-range interactions by plain cutoffs at 1.2 nm.

The hybrid QM/MM-MD simulations were initiated from the fully equilibrated structures obtained during classical MD simulations. A combination of the GROMACS (for MD calculations) and ORCA 2.9[40] (for QM calculations) packages was applied. The QM part of the system contained the F4G molecule and the corresponding interactions were computed within the BP86/def2-SVP[41,42] potential. The MM part comprised water molecules (TIP3P model). The interactions at the QM/MM interface were computed according to the electronic embedding scheme[43] and the CHARMM/TIP3P non-bonded parameters analogous to those used during classical MD simulations. The equations of motion were integrated with a time step of 0.5 fs without any constraints on bond lengths or valence angles of solute molecules. The non-bonded interactions were computed by using plain cutoffs at 1.2 nm. The box volume was fixed,

keeping the volume of the simulation box constant. The MD simulations were carried out for a duration of 100 ps and the trajectory was saved every 10 steps; other details corresponded to the setup of the classical MD simulations.

The values of the spectroscopic parameters ($^nJ_{CH}$ and $^nJ_{HH}$ coupling constants as well as ^1H and ^{13}C NMR chemical shifts)
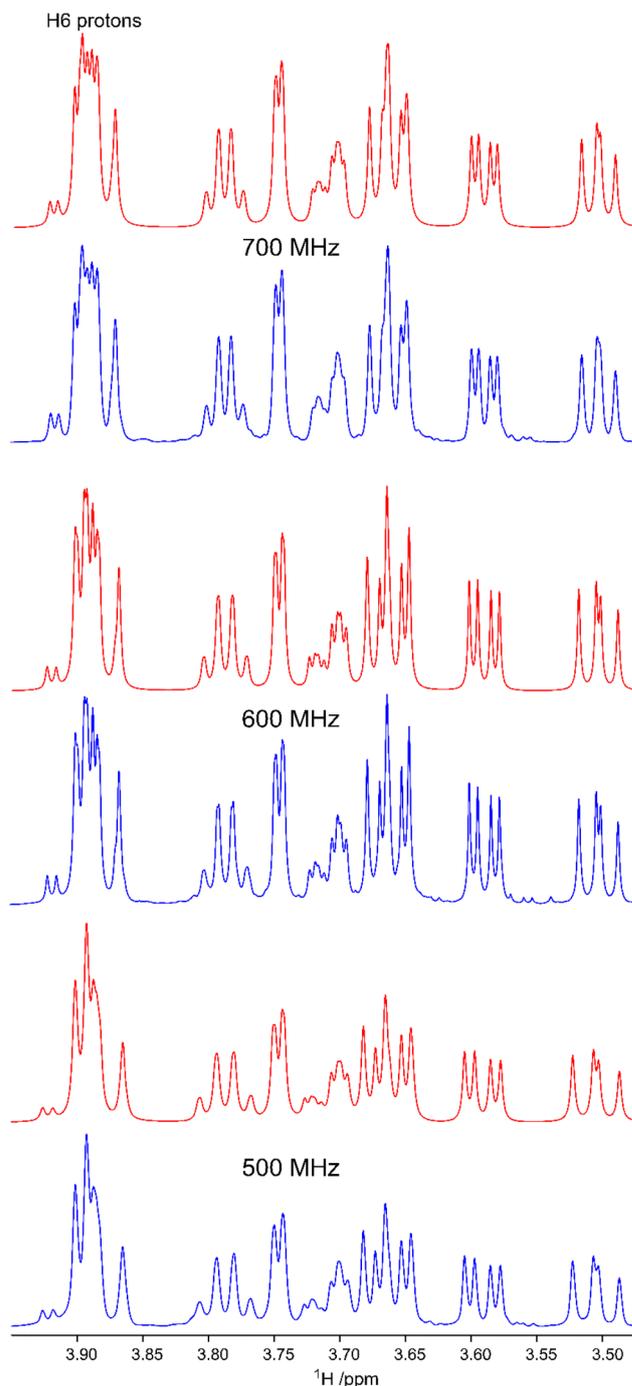

Fig. 2 Selected ^1H NMR spectral region of β-L-Fuc*p*-(1→4)-α-D-Glc*p*-OMe at 700 MHz (top), 600 MHz (middle) and 500 MHz (bottom). NMR spectra from experiments are presented in blue color and the corresponding ones obtained by NMR spin-simulation using PERCH are shown in red color.

6982 | *Org. Biomol. Chem.*, 2023, **21**, 6979–6994

This journal is © The Royal Society of Chemistry 2023

Table 1 ^{1}H NMR chemical shifts (ppm) of β-L-Fucp-(1→4)-α-D-Glcp-OMe in D$_2$O at 306 K refined by NMR spin-simulation using PERCH and averaged from NMR spectra at 500, 600 and 700 MHz; standard deviations <0.001 ppm. ^{13}C NMR chemical shifts (ppm) of the disaccharide in D$_2$O at 343 K.[11] Chemical shifts were calculated from isotropic nuclear magnetic shielding constants as described in Materials and methods

Proton	[1]H expt.	[1]H calc.	Carbon	[13]C expt.	[13]C calc.
H1′	4.645	4.755	C1′	104.40	102.77
H2′	3.506	3.511	C2′	72.16	72.99
H3′	3.659	3.481	C3′	73.84	74.27
H4′	3.747	3.726	C4′	72.13	72.74
H5′	3.787	3.807	C5′	71.78	72.81
H6′	1.265	1.317	C6′	16.15	16.42
H1	4.817	4.838	C1	100.06	99.37
H2	3.592	3.538	C2	72.08	73.40
H3	3.883	3.931	C3	73.87	75.28
H4	3.666	3.706	C4	78.46	75.99
H5	3.708	3.692	C5	71.10	72.23
H6$_{pro-R}$	3.904	3.766	C6	61.62	61.95
H6$_{pro-S}$	3.884	3.885			
OMe[a]	3.424	3.534	OMe	55.98	53.37

[a] Averaged over the three protons in the methyl group of the fucosyl residue.

were calculated by adopting the multi-step protocol proposed by Gaweda and Plazinski[44] and according to the protocol used in our previous study.[45] In the first step, the unbiased explicit solvent MD simulations within the classical force field were carried out according to the protocol described above. The analysis of the MD trajectory provided information about the possible conformers of the F4G molecule and their corresponding populations. In the next step, the most populated

conformers were extracted from the trajectory and subjected to *ab initio*-based geometry optimization in the presence of implicit, aqueous solvent. For each of the fully optimized structures the spectroscopic NMR parameters (*P*) were calculated. The final, averaged values of any *P* were calculated according to the following equation:

$$P = \frac{\sum_{i}^{N} p_i P_i}{\sum_{i}^{N} p_i}, \tag{5}$$

where $P = {}^nJ_{CH}$, ${}^nJ_{HH}$, δ_C or δ_H, p_i is the population of the *i*th conformer, according to the MD simulations, P_i is the corresponding *P* parameter value and *N* = 400 is the number of considered structures. Alternatively, in some cases, we used a modified version of eqn (5), in which p_i was calculated directly from QM energies by using the Boltzmann weights. In addition, eqn (5) was used to calculate the average conformational energies upon replacing P_i by the QM energy of the *i*th molecular configuration. In any calculation concerning distinct conformers and eqn (5), molecular configurations were filtered by using geometrical criteria ascribing them to particular conformational states and the *N* value was modified accordingly.

The values of chemical shifts (δ_i) were calculated from isotropic nuclear magnetic shielding constants (σ) by assuming a linear relation:[46]

$$\delta_i = \sigma_{ref} - \sigma_i, \tag{6}$$

Table 2 NMR proton–proton cross-relaxation rates of β-L-Fucp-(1→4)-α-D-Glcp-OMe in D$_2$O at 600 MHz and 318 K employing 1D ^{1}H,[1]H-NOESY experiments, derived proton–proton distances, hetero- and homonuclear scalar coupling constants, and computed data from MD simulations

Atom pair	$\sigma \times 10^2$ (s^{-1})	r_{expt}[a] (Å)	r_{MD}[b] (Å)	r_{MD}[n] (Å)	r_{MD}[o] (Å)	r_{MD}[p] (Å)
H1′,H4	6.76[c]	2.382	2.385	2.382	3.676	3.633
H1′,H3	0.95	3.303	3.688	3.747	2.463	4.249
H1′,H2′	1.71	2.995	3.056	3.056	3.058	3.057
H1,H2	6.41	2.403[d]	2.403[d]	2.403	2.421	2.398

	Method	$^3J_{expt}$ (Hz)	$^3J_{MD}$ (Hz)	$^3J_{MD+QM}$[j] (Hz)	$^3J_{MD+QM}$[k] (Hz)	$^3J_{QM/MM-MD}$ (Hz)
H1′,C4	J-HMBC	4.00	3.13[e]	2.97	4.30	3.14[l]
	1DLR	3.74				
C1′,H4	J-HMBC	5.30	5.63[f]	6.42	6.88	5.66[m]
	1DLR	5.22				

	Method	$^3J_{expt}$ (Hz)	$^3J_{MD}$ (Hz)	$^3J_{MD+QM}$[j] (Hz)	$^3J_{MD+QM}$[k] (Hz)
H5,H6$_{pro-R}$	PERCH	4.55 (0.03)[i]	4.95[g]	5.51	3.85
H5,H6$_{pro-S}$	PERCH	2.24 (0.09)[i]	2.27[h]	2.42	2.53

[a] Calculated according to $r_{ij} = r_{ref}(\sigma_{ref}/\sigma_{ij})^{1/6}$. [b] Calculated as $r_{MD} = \langle r^{-6} \rangle^{-1/6}$ over the whole trajectory. [c] Obtained from $\sigma_{H1',H3'+H4} = 0.117$ s^{-1}, an effective distance $r_{H1',H3'} = 2.510$ Å from MD simulation and rearrangement of the ISPA formula to give $\sigma_{ij} = \sigma_{ref}(r_{ref}/r_{ij})$,[6] *i.e.*, $\sigma_{H1',H3'} = 4.94 \times 10^{-2}$ s^{-1}. [d] Reference distance. [e] Scalar coupling constants were calculated from MD simulation using eqn (1). [f] Scalar coupling constants were calculated from MD simulation using eqn (2). [g] Scalar coupling constants were calculated from MD simulation using eqn (3). [h] Scalar coupling constants were calculated from MD simulation using eqn (4). [i] Standard deviation. [j] QM calculations using 400 MD-extracted frames with constraints on glycosidic linkage; weighted according to MD populations. [k] QM calculations using 400 MD-extracted frames with constraints on glycosidic linkage; weighted according to QM energies. [l] Eqn (1), QM/MM-MD simulations. [m] Eqn (2), QM/MM-MD simulations. [n] Calculated as $r_{MD} = \langle r^{-6} \rangle^{-1/6}$ for *syn*-conformations. [o] Calculated as $r_{MD} = \langle r^{-6} \rangle^{-1/6}$ for *anti-ψ* conformations. [p] Calculated as $r_{MD} = \langle r^{-6} \rangle^{-1/6}$ for *anti-φ* conformations.

where σ_{ref} is a reference value, treated here as an adjustable parameter, common for the whole set of δ_i values.

The QM calculations were performed in Gaussian09[47] at the DFT/B3LYP/6-311+G(d,p) level of theory[48,49] and in the presence of implicit, aqueous solvent (polarizable continuum model).[50] The geometry optimization was performed by using the default criteria, except for the use of the *tight* keyword, tightening the cutoffs on forces and step size. Subsequently, spectroscopic parameters were calculated for the fully optimized structures using the GIAO (gauge-independent atomic orbital) approach[51] at the same level of theory. The *mixed* keyword was invoked to request a two-step spin–spin coupling calculation.[52] Independently, in order to determine the dependence of the $^3J_{\text{CH}}$ coupling constants on a broader range of the ϕ and ψ values, the QM-based optimization and calculation of the NMR parameters were repeated for the same set of structures but with either ϕ or ψ constrained with respect to their initial, MD-derived, values.

Results and discussion

In the study describing the synthesis of β-L-Fuc*p*-(1→4)-α-D-Glc*p*-OMe the ^{1}H and ^{13}C NMR chemical shifts were assigned for the disaccharide in D$_2$O solution at elevated temperatures of 358 K and 343 K, respectively,[11] as higher temperatures are beneficial in structural studies of polysaccharides, both with respect to displacement of the residual HDO peak from the spectral region where resonances from anomeric protons reside and for NMR line shapes, facts that were important in the development of computer-assisted spectrum analysis of polysaccharides at that time.[53] Certain ^{1}H NMR chemical shifts showed spectral overlap and the H6 protons of the hydroxymethyl group in the glucosyl residue were degenerate, precluding a straightforward conformational analysis of the rotamer distribution of the ω torsion angle of the exocyclic

group. As a basis for the conformational analysis of F4G, ^{1}H NMR experiments were carried out at a lower temperature of 306 K and, in particular, one-dimensional ^{1}H NMR spectra were obtained at three magnetic field strengths corresponding to ^{1}H NMR frequencies of 500, 600 and 700 MHz (Fig. 2). The ^{1}H chemical shifts of F4G were refined by NMR spin-simulation[14] (Table 1) and as the procedure fits spectral data containing information on both chemical shifts and spin–spin coupling constants, also $^nJ_{\text{HH}}$ are determined once agreement between experimental and simulated spectra has been obtained (Fig. 2). Although the ^{1}H NMR chemical shifts of the protons of the hydroxymethyl group in the glucosyl reside are closely similar they could be differentiated, resulting in 3.904 ppm and 3.884 ppm, with $^3J_{\text{H5,H6}}$ of 4.55 Hz and 2.24 Hz
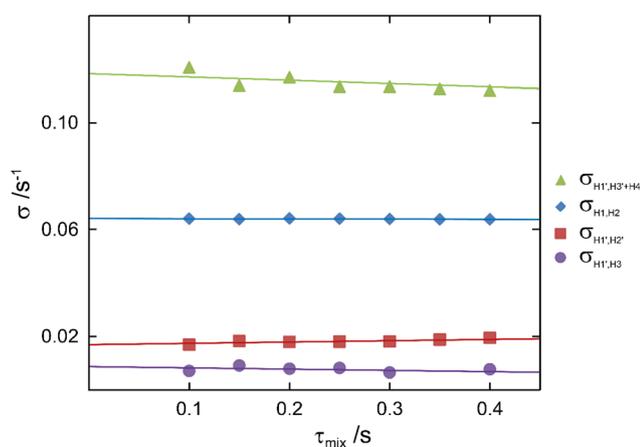

Fig. 3 Plots of $-I_j(\tau_{\text{mix}})/[\tau_{\text{mix}}I_i]$ *versus* τ_{mix} for 1D ^{1}H,^{1}H-NOESY NMR experiments at 600 MHz of β-L-Fuc*p*-(1→4)-α-D-Glc*p*-OMe. Proton–proton interactions: H1',H3' + H4 (triangles), H1,H2 (diamonds), H1',H2' (squares) and H1',H3 (circles).
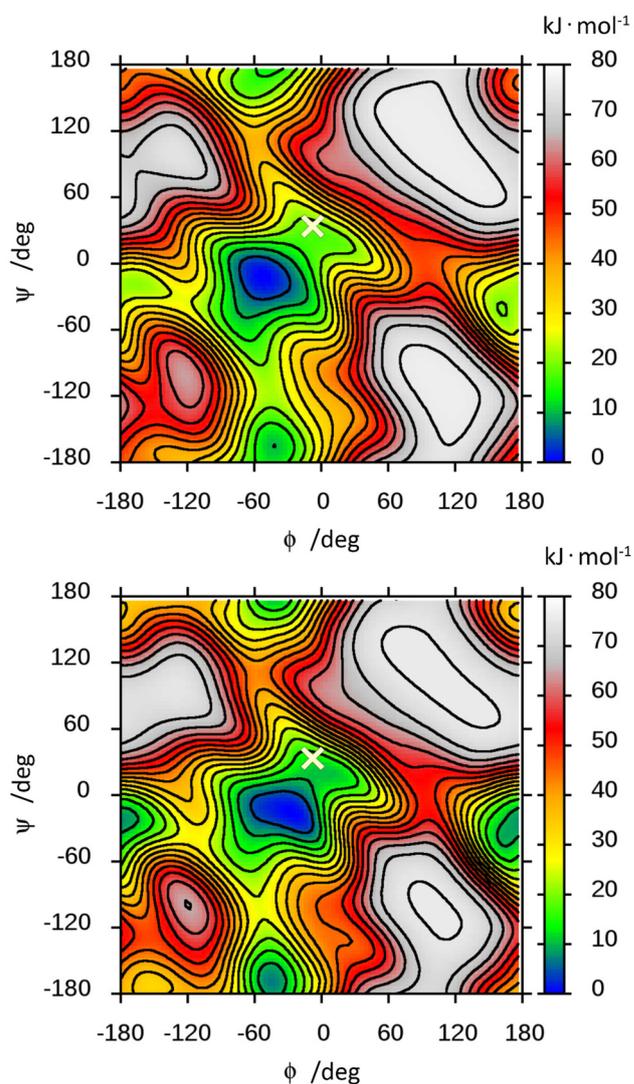

Fig. 4 Free energy landscape of β-L-Fuc*p*-(1→4)-α-D-Glc*p*-OMe calculated from MD simulations (metadynamics protocol) carried out in the presence of explicit water (top) and *in vacuo* (bottom). The glycosidic torsion angles are ϕ = H1'–C1'–O4–C4 and ψ = C1'–O4–C4–H4 and the conformation described by these in the crystal structure is marked by a cross (×) at $\phi = -6°$ and $\psi = 34°$.

6984 | *Org. Biomol. Chem.*, 2023, **21**, 6979–6994

This journal is © The Royal Society of Chemistry 2023

(Table 2), respectively. Based on $^3J_{H5,H6}$ observed in glucopyranosyl residues[10] the resonances were assigned to $H6_{pro-R}$ and $H6_{pro-S}$, respectively, which will be further supported in the subsequent conformational analysis (*vide infra*). Moreover, the ^1H NMR chemical shift of H4 in Glc was 3.666 ppm and for H3′ in Fuc it was 3.659 ppm, *i.e.*, a chemical shift difference of <0.01 ppm.

The conformational space populated by F4G was investigated using a combination of NMR experiments and computational methods. Proton–proton cross-relaxation rates across the glycosidic linkage between the two sugar residues as well as those from intra-residue correlations were obtained by 1D $^1H,^1H$-NOESY and $^1H,^1H$-STEP-NOESY experiments. An array of mixing times utilizing selective excitations at the resonance frequencies for anomeric protons, as well as a TOCSY spin-lock for transfer from H1 to H3 followed by selective excitation in the latter experiment, resulted in NOE buildup curves that were analyzed as devised by Dixon *et al.*[19] (Fig. 3), whereby proton–proton cross-relaxation rates were obtained (Table 2). From the MD simulation an effective distance for the H1,H2 pair in the α-linked glucosyl residue was calculated as 2.40 Å and used as a reference distance to obtain information on inter-residual proton–proton interactions. For the β-linked fucosyl residue the H1′,H2′ distance obtained from experiment using ISPA resulted in a longer distance of 3.00 Å in good agreement with that from the MD simulation, being 3.06 Å. The severe spectral overlap of H4 in Glc and H3′ in Fuc precluded direct analysis of the transglycosidic H1′,H4 NOE. However, its cross-relaxation rate and subsequently the distance between H1′ and H4 could be obtained following the procedure described by Zaccheus *et al.*,[54] *i.e.*, the computed effective intra-residue H1′,H3′ distance being 2.51 Å from the MD simulation was together with rearrangement of the ISPA formula used to give the cross-relaxation rate for H1′,H3′, which was subtracted from the sum of the two contributions to the determined cross-relaxation rate (Table 2) from the buildup of the NOE peak at ~3.66 ppm. The transglycosidic H1′,H4 distance was from the NOE experiment determined to

Table 3 Hydrogen bonding occurrences (%) within β-L-Fuc*p*-(1→4)-α-D-Glc*p*-OMe according to MD simulations with explicit water molecules as solvent

Donor	Acceptor	MD (additive FF)	QM/MM-MD
HO3	O5′	0.5	0
HO3	O5′	80.6[a]	—
HO3	O5′	47.4[b]	—
HO6	O5′	51.4[c]	98.2[d]
HO3	HO2′	3.2	0
HO6	HO2′	0.1	0

[a] Determined exclusively for *anti-φ* conformation. [b] Determined exclusively for *anti-ψ* conformation. [c] Distribution of the O5′···HO6 hydrogen bond: *gt* = 0%, *gg* = 85% and *tg* = 15%. [d] *gt* = 0%, *gg* = 100% and *tg* = 0%.

be 2.38 Å, in excellent agreement with that from the MD simulation, also being 2.38 Å.

The free energy landscape of F4G was computed from the MD simulations in the presence of explicit water and *in vacuo* (Fig. 4). The low-energy region is observed for an *exo-syn* conformation in which the ϕ torsion angle shows an *exo-anomeric* conformation and the ψ torsion angle is tilted to some extent from an eclipsed conformation; thus, the hydrogen atoms at the glycosidic linkage are arranged such that they are on the same side of a plane perpendicular to the C1′,H1′ bond. The MD simulation showed for glycosidic torsion angles averages and root-mean-square deviations (in parentheses) of $\langle\phi\rangle$ = −52.1° (13.4), $\langle\psi\rangle$ = −14.6° (18.5) and $\langle\phi_{Me}\rangle$ = −50.0° (11.1) with explicit water molecules as solvent. The free energy landscape of F4G calculated from this set of MD simulations shows, besides the major *syn*-conformation centered at $\phi/\psi \approx$ −50°/−15°, that two *anti*-conformational states are populated, *anti-φ* and *anti-ψ*, with a closely similar free energy surface of the *in vacuo* ϕ/ψ map (Fig. 4). Although the crystal structure of F4G corresponds to a *syn*-conformation with ϕ = −6° and ψ = 34°, this conformation corresponds to a free energy difference of ~20 kJ mol^{-1}, suggesting that intermolecular forces (crystal
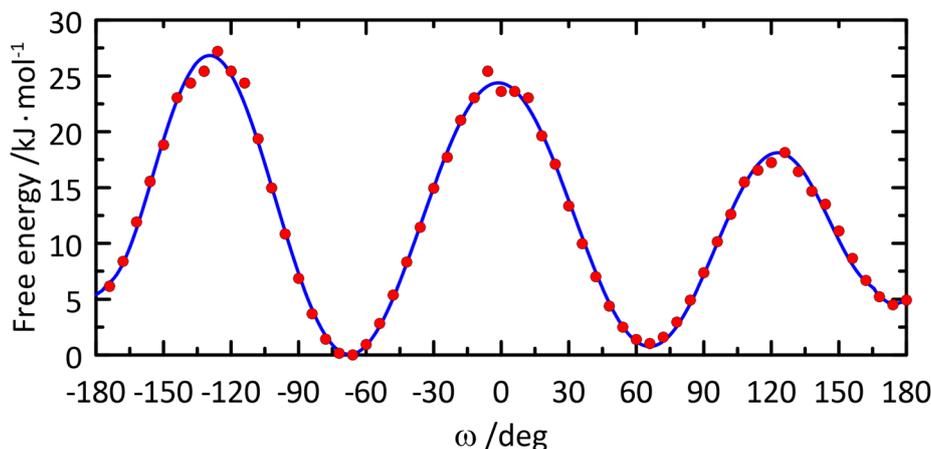

Fig. 5 Free energy profile of the ω torsion angle in the glucosyl residue of β-L-Fuc*p*-(1→4)-α-D-Glc*p*-OMe.
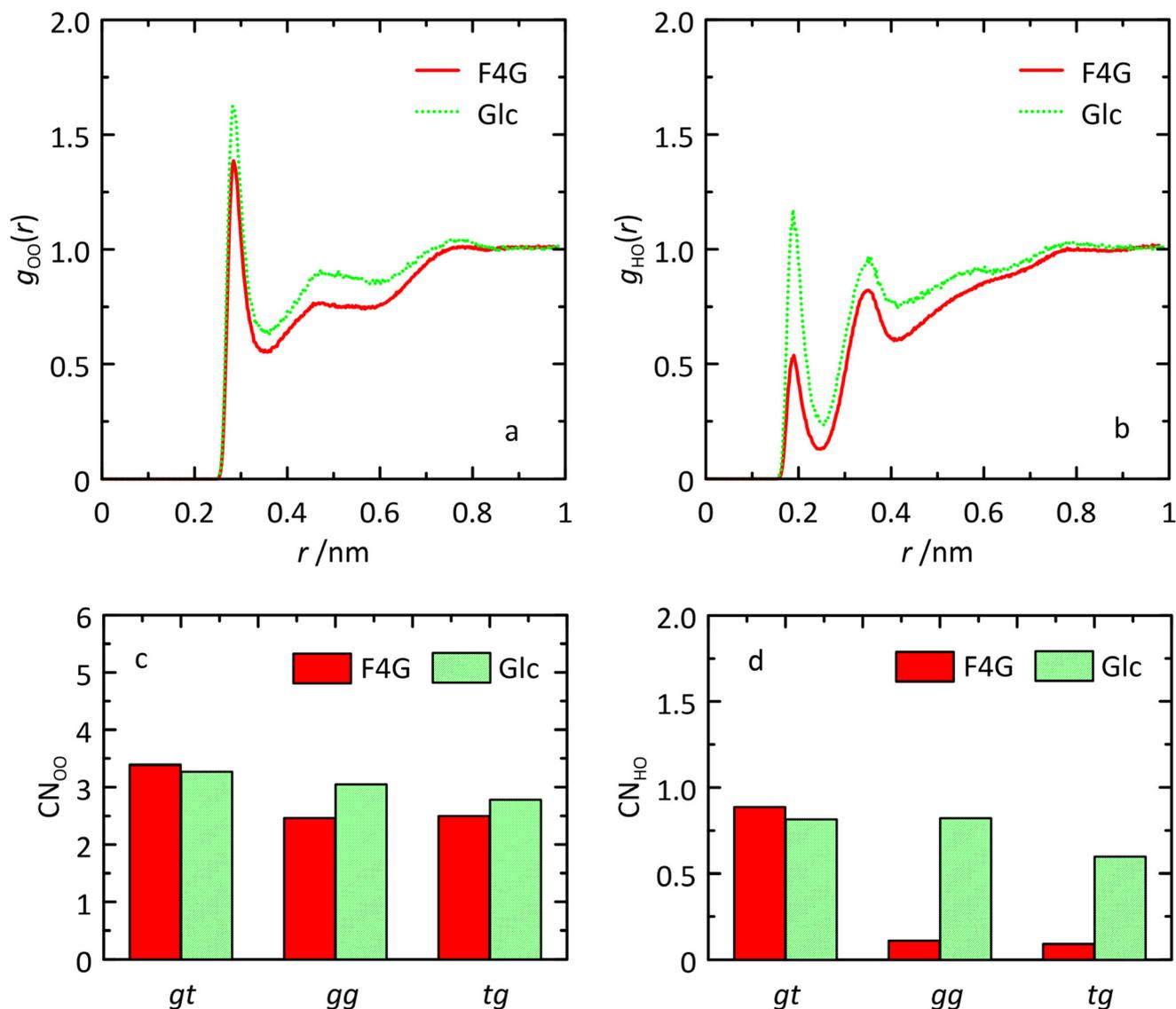
Fig. 6 Radial distribution functions $g_{OO}(r)$ and $g_{HO}(r)$ of O6 (a) and HO6 (b) atoms of the hydroxymethyl group to oxygen atoms in water molecules in β-L-Fuc$p$-(1→4)-α-D-Glc$p$-OMe and α-D-Glc$p$-OMe, and the obtained coordination numbers for the three conformational states gt, gg and tg related to O6 (c) and HO6 (d). Coordination numbers were calculated using the cutoff values of 0.35 and 0.25 nm for O6 and HO6, respectively.

packing) affect the conformation of the disaccharide in the solid state to a significant extent. However, for the α-D-hexopyranoside at the reducing end of the disaccharide the *exo*-

Table 4 Effective proton–proton distances (Å) for the three rotamers of the ω torsion angle in β-L-Fuc$p$-(1 → 4)-α-D-Glc$p$-OMe from MD simulations averaged as $r_{MD} = \langle r^{-6} \rangle^{-1/6}$ over the trajectory

Atom pair	r_{MD} (gt)	r_{MD} (gg)	r_{MD} (tg)
HO6,H4	4.337	2.344	2.964
HO6,H1′	6.044	3.500	3.477
HO6,H5′	6.849	3.556	3.921
HO6,H6″[a]	6.040	2.898	3.474

[a] Averaged over the three protons in the methyl group of the fucosyl residue.

anomeric conformation is maintained with $\phi_{Me} = -56°$, closely similar to the average conformation from the MD simulations.

The local minima of the free energy corresponding to the *anti-ψ* and *anti-φ* conformers have levels of 9.9 and 19.2 kJ mol^{-1} with respect to the *exo-syn* conformation, respectively. This corresponds to the *exo-syn* : *anti-ψ* : *anti-φ* distribution of *ca.* 98 : 2 : 0, respectively. Similar energy levels (10.2 and 13.6 kJ mol^{-1}, respectively) and roughly identical distribution of conformational states (98 : 2 : 0, respectively) are obtained when calculating the average energies of particular conformers of the glycosidic linkage by using the QM data and the modified version of eqn (5) in which spectroscopic parameter values P_i are replaced by QM energies.

Flexibility at the glycosidic linkage of oligosaccharides has been identified as *anti*-conformations at both the ϕ and ψ

6986 | *Org. Biomol. Chem.*, 2023, **21**, 6979–6994

This journal is © The Royal Society of Chemistry 2023

torsion angles.[55–58] A comparison of the experimental distance from the NOESY experiments shows H1′,H3 = 3.30 Å, which is shorter than the effective distance computed from the MD simulation for which H1′,H3 = 3.69 Å. Furthermore, the effective distance for the all-*syn*-conformation is 3.75 Å, whereas averaged over the *anti*-ψ conformational state it is significantly shorter, being 2.46 Å (Table 2). Thus, to investigate to what extent the *anti*-ψ conformational state is populated, NMR data from the 1D ^{1}H,^{1}H-NOESY experiments of the interaction between protons together with computed distances from the MD simulation can be used in a two-state analysis, *e.g.*, *syn*- and *anti*-conformation at the glycosidic linkage:

$$(1-x)\langle r_{syn}^{-6}\rangle + (x)\langle r_{anti}^{-6}\rangle = r_{expt}^{-6} \qquad (7)$$

where x is the fraction that populates the *anti*-conformation. Rearrangement of eqn (7) leads to:

$$x = \frac{r_{expt}^{-6} - r_{syn}^{-6}}{r_{expt}^{-6} - r_{syn}^{-6}} \qquad (8)$$

from which the degree of the *anti*-conformation can be determined. It is judged that population of the *anti*-ϕ conformational state does not contribute to any significant extent to a shorter H1′,H3 distance as the computed distance H1′,H3 = 4.25 Å, *i.e.*, even longer than for the *syn*-conformation. Application of the experimentally determined and computed distances using eqn (8) leads to $x = 0.10$ for F4G in water solution, *i.e.*, the amount of *anti*-ψ conformation is small, but its presence is supported by the experimental NMR data, consistent with the free energy surface obtained from the MD simu-
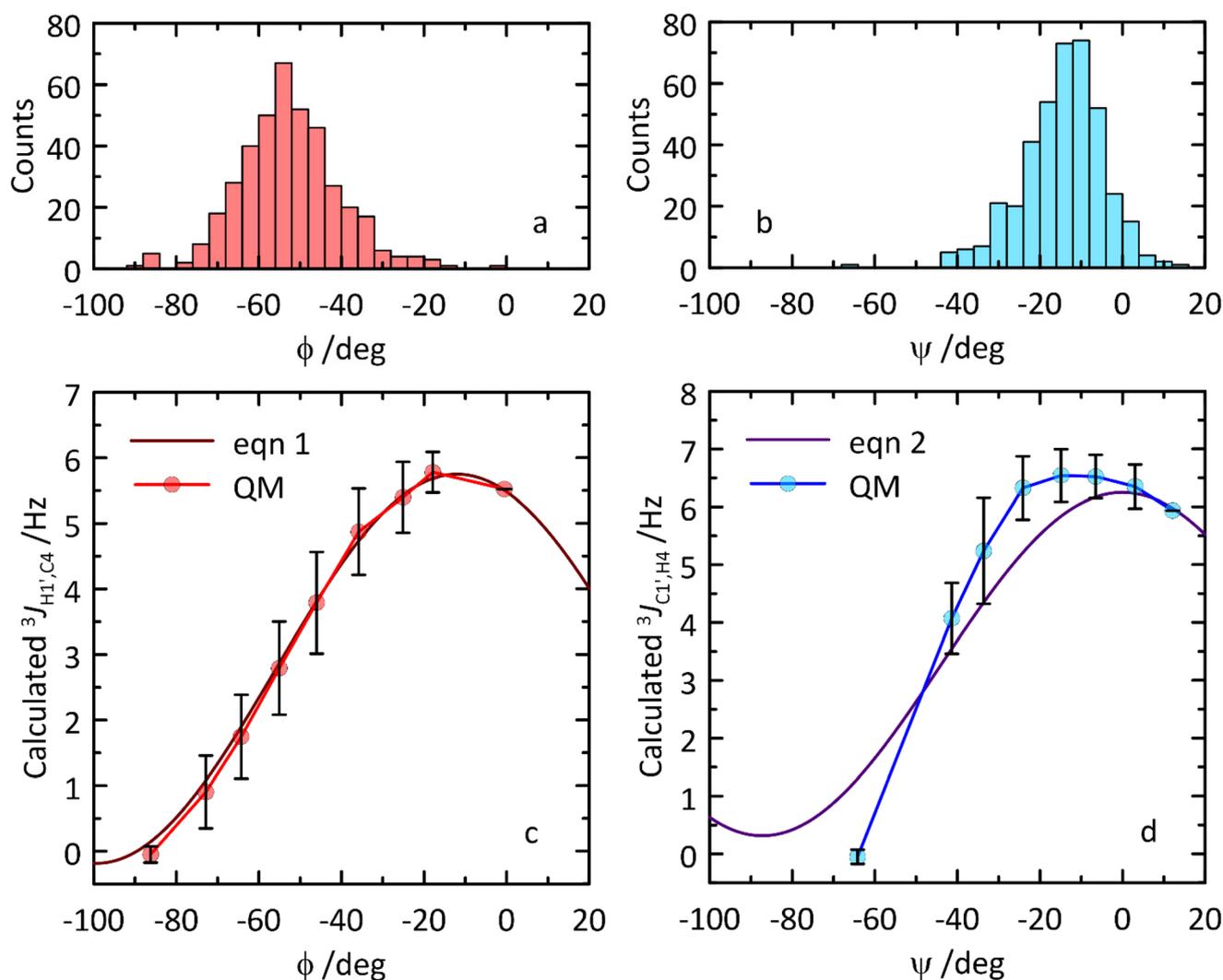

Fig. 7 (a and b) Distribution of ϕ and ψ torsion angle values across the subsampled ensemble of 400 MD structures. (c and d) Comparison of trans-glycosidic $^3J_{CH}$ Karplus-type relationships (eqn (1) and (2)) (solid lines) for the ϕ and ψ torsion angles in β-L-Fuc*p*-(1→4)-α-D-Glc*p*-OMe to those calculated using constrained torsion angles from MD simulations and subsequently QM-based geometry-optimized structures (circles). QM data correspond to the averages calculated within 10° ranges. Vertical bars denote the corresponding standard deviation values.

lation and the QM calculations. In addition, a calculation based on the effective transglycosidic distances for H1′,H4 from the MD simulation of the *syn*-conformation and the *anti-ψ* conformation (Table 2 and eqn (7)) reveals that the effective H1′,H4 distance for a population equilibrium where the *anti-ψ* conformation is present to 10% leads to an increase of the H1′,H4 distance by only 0.04 Å, which is still in very good agreement with the experimental data for this proton–proton interaction.

The free energy profile of the ω torsion angle was computed from the MD simulation (Fig. 5) and the rotamer distribution for *gt* : *gg* : *tg* was 39 : 52 : 9, respectively, in excellent agreement with that obtained from NMR $^3J_{H5,H6}$ coupling constants (Table 2) resulting in, for the rotamers, *gt* : *gg* : *tg* of 38 : 53 : 9, respectively, similar to that of α-D-Glc*p*-OMe having the *gt* : *gg* : *tg* rotamers populated as 42 : 49 : 9, respectively.[59] If the ^{1}H NMR resonance assignments for the hydroxymethyl protons in F4G were to be reversed, with a small coupling constant for H5,H6$_{pro-R}$ and a large coupling constant for H5, H6$_{pro-S}$, this would lead to a rotamer distribution for *gt* : *gg* : *tg* of 2 : 64 : 34, respectively, which disagrees with the one obtained from the MD simulation in particular, and glucopyranosyl residues in general.[10,60] It may be noted that the average values the glycosidic torsion angles ϕ and ψ are closely similar even if the ω conformational state is altered, *i.e.*, $\langle\phi\rangle_{gt}$ = −51.7°, $\langle\psi\rangle_{gt}$ = −16.5°, $\langle\phi\rangle_{gg}$ = −53.3°, $\langle\psi\rangle_{gg}$ = −13.8°, $\langle\phi\rangle_{tg}$ = −47.0°, and $\langle\psi\rangle_{tg}$ = −11.4°.

Analysis of the MD simulation revealed that inter-residue hydrogen bonding occurred to a significant extent: for O5′···HO6 in the *syn*-conformation to ~50% and for O5′···HO3 in both the *anti-φ* and *anti-ψ* conformational states to ~80% and ~50%, respectively (Table 3). A large upfield chemical shift

displacement, $\Delta\delta_H \approx -0.5$ ppm, for HO6 in F4G compared to α-D-Glc*p*-OMe has been reported and the shielding of the proton was attributed to its proximity to O5′ in the fucosyl residue.[61,62] The result from the MD simulation showing the occurrence of the O5′···HO6 hydrogen bond during half of the time and consequently reduced hydration can be further analyzed using radial distribution functions (RDFs) $g_{OO}(r)$ and $g_{HO}(r)$ and coordination numbers (CNs).[63,64] The RDFs of the HO6 atoms to oxygen atoms in water molecules are for O6 in F4G quite similar to those for O6 in α-D-Glc*p*-OMe and so are the CNs (Fig. 6). For F4G in which the hydroxymethyl group populates the conformational states *gg* and *tg* the RDF CN$_{OO} \approx 2.5$, whereas in the *gt* state CN$_{OO} \approx 3.4$. In contrast, analysis of the RDF and CN for the hydrogen atom of the hydroxymethyl group showed reduced hydration (Fig. 6) with CN$_{HO}(r) \approx 0.1$ in the *gg* and *tg* states compared to CN$_{HO}(r) \approx 0.9$ in the *gt* state, a finding in agreement with the interpretation based on the upfield ^{1}H NMR chemical shift displacement.

Notably, it is for the *gg* rotamer that the O5′···HO6 hydrogen bond is of greatest importance. When this hydrogen bonding takes place, it is distributed such that 85% of the time the hydroxymethyl group populates the *gg* conformational state but only 15% of the time is the *tg* conformational state involved (Table 3). ^{1}H,^{1}H-NOEs have been reported between HO6 and H4 on the glucosyl residue and inter-residually from HO6 to H1′, H5′ and H6′.[61] NOEs are weighted according to an $\langle r_{ij}^{-6}\rangle$-average and the effective distances were calculated from the MD simulation (*vide supra*) for the four inter-proton interactions; whereas the HO6,H1′ distance was similar in both the *gg* and *tg* rotamers, those between HO6 and H4, H5′ and H6′ were all shorter for the *gg* rotamer than for the *tg* rotamer
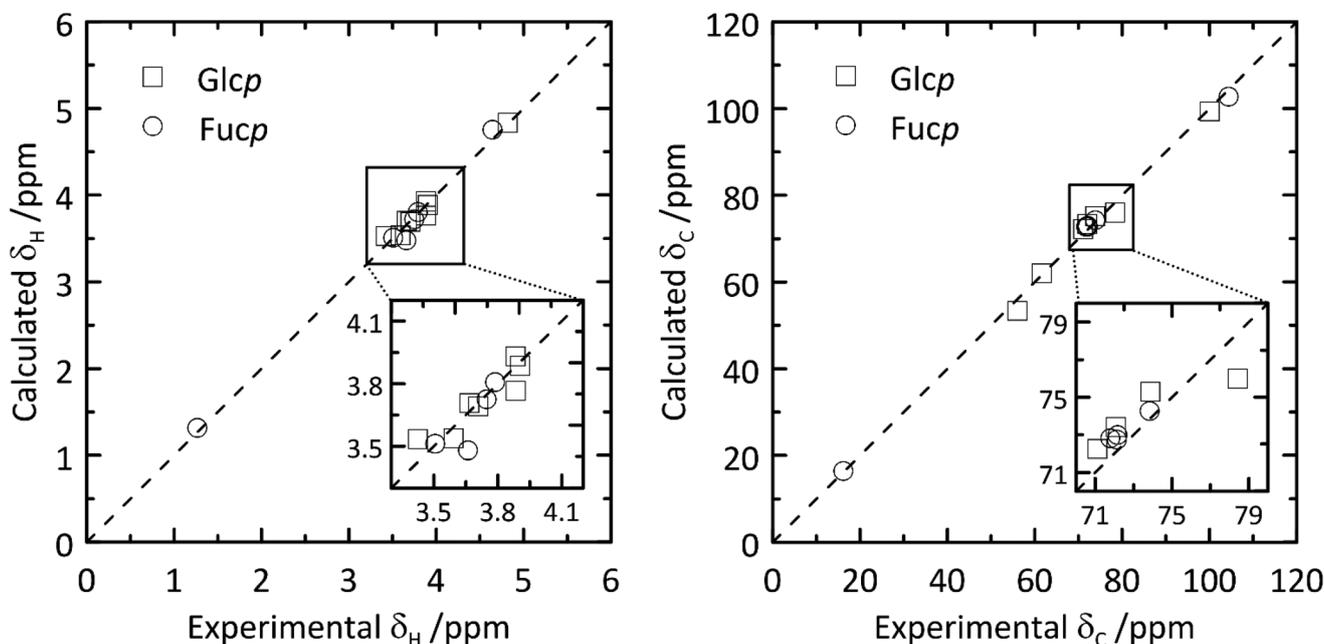

Fig. 8 Calculated *versus* experimental ^{1}H (left) and ^{13}C (right) NMR chemical shifts of β-L-Fuc*p*-(1→4)-α-D-Glc*p*-OMe.[11]

6988 | *Org. Biomol. Chem.*, 2023, **21**, 6979–6994

This journal is © The Royal Society of Chemistry 2023

(Table 4), which may also be consistent with the NOEs previously observed.

Barriers to rotation of the ω torsion angle from the 1D free energy (F) profile (Fig. 5) were calculated from the classical MD simulation and a polynomial curve fitting of degree 12 resulting in: $\Delta F(gt \to gg) = 23.5$ kJ mol^{-1}, $\Delta F(gt \to tg) =$ 17.3 kJ mol^{-1}, $\Delta F(gg \to gt) = 24.4$ kJ mol^{-1}, $\Delta F(gg \to tg) =$ 26.8 kJ mol^{-1}, $\Delta F(tg \to gg) = 22.3$ kJ mol^{-1}, and $\Delta F(tg \to gt) =$ 13.8 kJ mol^{-1}. The lowest barriers to rotation are related to transitions between the gt and tg conformational states, in which eclipsing of the O6 atom and the small H5 atom takes place. The two remaining barriers are associated with eclipsing
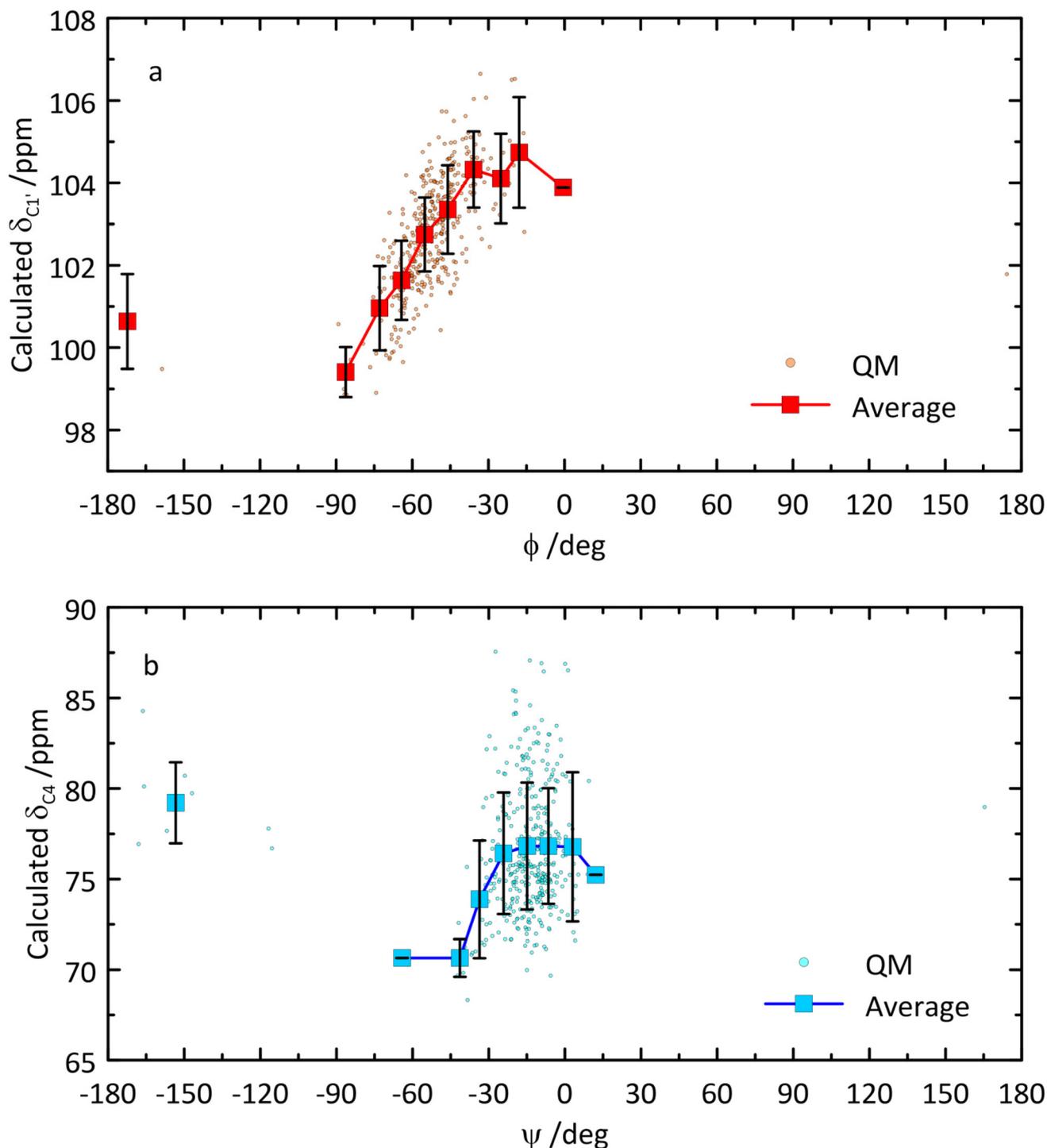

Fig. 9 Calculated ^{13}C NMR chemical shifts of C1' *versus* glycosidic torsion angle ϕ (a) and of C4 *versus* glycosidic torsion angle ψ (b) of β-L-Fuc*p*-(1→4)-α-D-Glc*p*-OMe.

This journal is © The Royal Society of Chemistry 2023

Org. Biomol. Chem., 2023, **21**, 6979–6994 | **6989**

of O6 with either O5 or C4, *i.e.*, much larger atoms, which results in stronger repulsive interactions and, consequently, higher barriers for rotation. This effect is accompanied by the influence of the O5′⋯HO6 hydrogen bond, which is pronounced when the hydroxymethyl group in the glucosyl residue has the *gg* conformation. Thus, the *gg* → *gt* and *gg* → *tg* barriers are presumably elevated by the energy needed to disrupt this interaction. The independent MD simulations of α-D-Glc*p*-OMe (carried out according to a protocol identical to that applied for F4G), demonstrated that all barriers to rotation of the ω torsion angle are reduced in comparison to F4G by 2.2–3.3 kJ mol⁻¹. In the context of barriers vicinal to the *gg* conformational state the effect of lowering barriers to rotation may be ascribed to lack of an intramolecular hydrogen bond involving HO6 when ω has the *gg* conformation. The rotamer distribution determined from MD simulations for α-D-Glc*p*-OMe is: *gt* : *gg* : *tg* = 42 : 55 : 3, *i.e.*, closely similar to that of F4G and in line with the NMR-based estimations.[59] The reduced population of the *tg* conformer in the monosaccharide may be attributed to more unfavorable interactions of O6 with O4, bearing a larger negative charge in comparison to O4 as part of the glycosidic linkage joining the two sugar residues in F4G (−0.65 *vs.* −0.36 *e*⁻, respectively).

Transglycosidic $^3J_{H1',C4}$ and $^3J_{C1',H4}$ coupling constants related to the glycosidic torsion angles ϕ and ψ, respectively, can *via* Karplus-type relationships give information of conformational preferences at the glycosidic linkage. Two different types of NMR experiments, J-HMBC and 1DLR,[20–22] were used to obtain heteronuclear coupling constants resulting in $^3J_{H1',C4}$ ≈ 4 Hz and $^3J_{C1',H4}$ ≈ 5 Hz related to the ϕ and ψ torsion angles, respectively. From the MD simulation heteronuclear coupling constants were computed using Karplus-type relationships (eqn (1) and (2), respectively) which underestimated $^3J(\phi)$ somewhat (Table 2), and in this case a parametrization[65] proposed by adding a phase shift Θ set as +6° to the originally proposed Karplus-type relationship (eqn (1)) resulted in 2.51 Hz, *i.e.*, an even larger deviation. In contrast, the computed $^3J(\psi)$ was instead somewhat overestimated from the MD

simulation (Table 2). An MD-based ϕ,ψ torsion angle distribution was sampled consisting of 400 structures (Fig. 7), which subsequently were constrained at specific torsion angles and geometry-optimized employing QM-based methodology. The computed $^3J_{H1',C4}$ coupling constants and the Karplus-type relationship for the ϕ torsion angle agree extraordinarily well, suggesting that this type of heteronuclear coupling constant at the glycosidic linkage can be used to assess carbohydrate force fields employed for MD simulations or to further refine force field parameters to obtain accurate descriptions of molecular structure and dynamics. Related to the ψ torsion angle, the QM-computed $^3J_{C1',H4}$ coupling constants are similar to those described by the Karplus-type relationship (Fig. 7) and the differences observed can be used for further improvement of the parametrization of the function (*i.e.*, of eqn (2)).

Interestingly, using eqn (1) and (2) in combination with QM/MM-MD trajectory leads to nearly the same $^3J_{H1',C4}$ and $^3J_{C1',H4}$ values as those determined from classical MD simulations (Table 2); the corresponding differences are marginal and do not exceed 0.03 Hz. This indicates that a quite accurate estimation of transglycosidic *J* coupling constants and the associated conformational properties is possible even when sampling of conformational space relies on very short (*i.e.*, of length of tens of ps) QM/MM-MD trajectories. Such observation may be relevant in the context of studying the conformation of rare sugars or saccharides with unusual substituents for which no thoroughly validated classical force fields are available. Still, the applicability of the QM/MM-MD simulations is restricted by the timescale of the conformational transitions relevant for the determined *J* coupling constants which can be illustrated by the case of $J_{H5,H6pro-R}$ and $J_{H5,H6pro-S}$; their values cannot be reliably estimated using the QM/MM-MD data, because the orientation of the hydroxymethyl moiety is conformationally restricted due to short sampling time.

The predictions made by the 'hybrid' approach relying on the use of MD-extracted structures, weighted accordingly and direct calculation of *J* coupling constants exhibit slightly larger
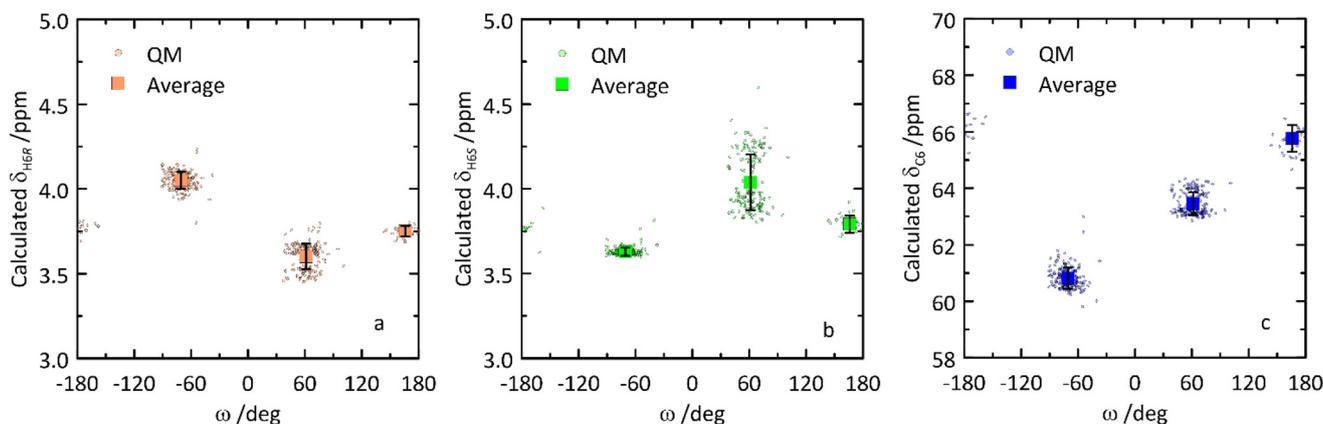

Fig. 10 Calculated NMR chemical shifts of H6$_{pro-R}$ (a), H6$_{pro-S}$ (b) and C6 (c) *versus* the ω torsion angle of the glucosyl residue in β-L-Fuc*p*-(1→4)-α-D-Glc*p*-OMe.

6990 | *Org. Biomol. Chem.*, 2023, **21**, 6979–6994

This journal is © The Royal Society of Chemistry 2023

deviations from the experimental values in comparison to the classical MD trajectories and eqn (1) and (2) (Table 2). This is a result of the lack of 'off-equilibrium' structures that do not correspond to either global or local energy minima in the set of structures subjected to QM calculations. This effect is a consequence of the geometry optimization procedure preceding calculations of the NMR parameters, which can influence the geometry of crucial degrees of freedom (such as ϕ and ψ torsion angles) and bias the average values of $^3J_{CH}$. However, the 'hybrid' approach still can be useful when applied to the cases of compounds for which no Karplus-like relationships are developed or to torsional angles displaying limited variability (e.g., convoluted into cyclic structure) and, therefore, less prone to geometry optimization-induced alterations of geometry. Replacing weights from MD populations by Boltzmann weights dependent only on the QM energies results in a significant improvement of the $^3J_{H1',C4}$ value but not that of $^3J_{C1',H4}$.

From the QM-based geometry-optimized ensemble ^1H and ^{13}C NMR chemical shifts were calculated at the DFT/B3LYP/6-311+G(d,p) level of theory. It is evident that for most NMR chemical shifts the agreement between experiment and computed data is very good (Table 1 and Fig. 8), using the population distribution from the MD simulation as the starting point for the calculation of chemical shifts. Furthermore, the conformational dependence of the ^{13}C NMR chemical shifts of the C1′ and C4 nuclei at the glycosidic linkage (Fig. 9) would make possible their use in refinement of the population distribution of the ϕ and ψ torsion angles. In addition, H6$_{pro-R}$ and H6$_{pro-S}$ show distinct ^1H NMR chemical shifts as a function of the conformational state of the ω torsion angle (Fig. 10) and although the ^1H chemical shift of H6$_{pro-R}$ differs between experiment and computed value, that of H6$_{pro-S}$ is in excellent agreement between experiment and computed value (Table 1). Moreover, for the three conformational states of the hydroxymethyl group the ^{13}C NMR chemical shift of C6 has a span of ~5 ppm, with the lowest chemical shift at ~61 ppm for the gg rotamer, at ~64 ppm for the gt rotamer and the highest chemical shift at ~66 ppm for the tg rotamer (Fig. 10). Convincingly, δ_{C6} agrees very well between experimental and computed values (Table 1), which supports the rotamer distribution for the ω torsion angle, and consequently the ^1H NMR chemical shift assignments for the hydroxymethyl protons (vide infra).

Conclusions

The conformational space at the glycosidic linkage of the disaccharide F4G is described by a low-energy region with an exo-syn conformation, present also in the crystal structure, and the two anti-ϕ and anti-ψ conformational states (Fig. 11). NMR spin-simulation of ^1H NMR spectra obtained at three different frequencies was used to refine chemical shifts, which for H6 protons of the hydroxymethyl group in the glucosyl residue differed by only 0.02 ppm, and homonuclear coupling constants that for $^3J_{H5,H6}$ in the glucosyl residue made it possible to determine the rotamer distribution of the ω torsion angle. In the major gg conformation for the hydroxymethyl group an O5′···HO6 hydrogen bond was highly populated as identified by MD simulations.

QM-based methodology facilitated the calculation of trans-glycosidic NMR $^3J_{CH}$ coupling constants and ^1H and ^{13}C NMR chemical shifts, the conformational dependence of the ^{13}C NMR chemical shifts at the glycosidic linkage, i.e., C1′ versus glycosidic torsion angle ϕ and C4 versus glycosidic torsion angle ψ, as well as the NMR chemical shifts of H6$_{pro-R}$, H6$_{pro-S}$ and C6 as a function of the ω torsion angle. The compu-

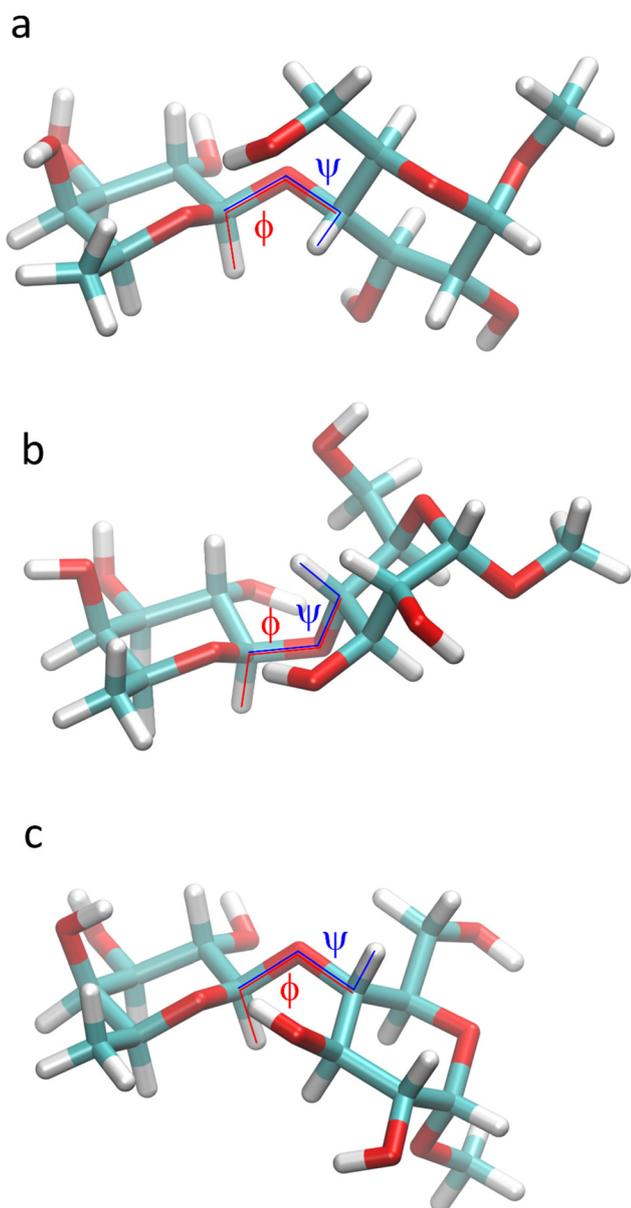**Fig. 11** Molecular models of β-L-Fucp-(1→4)-α-D-Glcp-OMe in which the two sugar residues are oriented such that they describe a syn-conformation (a), an anti-ϕ conformation (b) and an anti-ψ conformation (c) at the glycosidic linkage.

This journal is © The Royal Society of Chemistry 2023

Org. Biomol. Chem., 2023, **21**, 6979–6994 | **6991**

tational results show that the methodology developed based on MD simulations and QM calculations is able to accurately reproduce experimental NMR data.

Conflicts of interest

There are no conflicts to declare.

Acknowledgements

References

1 R. L. Schnaar, Glycobiology simplified: diverse roles of glycan recognition in inflammation, *J. Leukocyte Biol.*, 2016, **99**, 825–838.

2 B. A. H. Smith and C. R. Bertozzi, The clinical impact of glycobiology: targeting selectins, Siglecs and mammalian glycans, *Nat. Rev. Drug Discovery*, 2021, **20**, 217–243.

3 J. Y. Zhou and B. A. Cobb, Glycans in Immunologic Health and Disease, *Annu. Rev. Immunol.*, 2021, **39**, 511–536.

4 S. Esmail and M. F. Manolson, Advances in understanding N-glycosylation structure, function, and regulation in health and disease, *Eur. J. Cell Biol.*, 2021, **100**, 151186.

5 L. Eriksson and G. Widmalm, Crystal structure of methyl α-L-rhamnopyranosyl-(1→2)-α-L-rhamnopyranoside monohydrate, *Acta Crystallogr., Sect. E: Crystallogr. Commun.*, 2019, **75**, 854–857.

6 M. Zerbetto, A. Polimeno and G. Widmalm, Glycosidic linkage flexibility: The ψ torsion angle has a bimodal distribution in α-L-Rhap-(1→2)-α-L-Rhap-OMe as deduced from ^{13}C NMR spin relaxation, *J. Chem. Phys.*, 2020, **152**, 035103.

7 R. Pendrill, O. Engström, A. Volpato, M. Zerbetto, A. Polimeno and G. Widmalm, Flexibility at a glycosidic linkage revealed by molecular dynamics, stochastic modeling, and ^{13}C NMR spin relaxation: Conformational preferences of α-L-Rhap-(1→2)-α-L-Rhap-OMe in water and dimethyl sulfoxide solutions, *Phys. Chem. Chem. Phys.*, 2016, **18**, 3086–3096.

8 L. Eriksson, R. Stenutz and G. Widmalm, Methyl 4-O-β-L-fucopyranosyl α-D-glucopyranoside hemihydrate, *Acta Crystallogr., Sect. C: Cryst. Struct. Commun.*, 2000, **56**, 702–704.

9 E. R. Alonso, I. Peña, C. Cabezas and J. L. Alonso, Structural Expression of Exo-Anomeric Effect, *J. Phys. Chem. Lett.*, 2016, **7**, 845–850.

10 R. Stenutz, I. Carmichael, G. Widmalm and A. S. Serianni, Hydroxymethyl Group Conformation in Saccharides: Structural Dependencies of 2JHH, 3JHH, and 1JCH Spin–Spin Coupling Constants, *J. Org. Chem.*, 2002, **67**, 949–958.

11 I. Backman, B. Erbing, P.-E. Jansson and L. Kenne, N.m.r. and conformational studies of some 1,4-linked disaccharides, *J. Chem. Soc., Perkin Trans. 1*, 1988, 889–897.

12 M. Findeisen, T. Brand and S. Berger, A 1H-NMR thermometer suitable for cryoprobes, *Magn. Reson. Chem.*, 2007, **45**, 175–178.

13 R. Laatikainen, M. Niemitz, U. Weber, J. Sundelin, T. Hassinen and J. Vepsäläinen, General Strategies for Total-Lineshape-Type Spectral Analysis of NMR Spectra Using Integral-Transform Iterator, *J. Magn. Reson., Ser. A*, 1996, **120**, 1–10.

14 G. F. Pauli, S.-N. Chen, D. C. Lankin, J. Bisson, R. J. Case, L. R. Chadwick, T. Gödecke, T. Inui, A. Krunic, B. U. Jaki, J. B. McAlpine, S. Mo, J. G. Napolitano, J. Orjala, J. Lehtivarjo, S.-P. Korhonen and M. Niemitz, Essential Parameters for Structural Analysis and Dereplication by ^{1}H NMR Spectroscopy, *J. Nat. Prod.*, 2014, **77**, 1473–1487.

15 K. Stott, J. Keeler, Q. N. Van and A. J. Shaka, One-Dimensional NOE Experiments Using Pulsed Field Gradients, *J. Magn. Reson.*, 1997, **125**, 302–324.

16 H. Hu, S. A. Bradley and K. Krishnamurthy, Extending the limits of the selective 1D NOESY experiment with an improved selective TOCSY edited preparation function, *J. Magn. Reson.*, 2004, **171**, 201–206.

17 R. Pendrill, E. Säwén and G. Widmalm, Conformation and Dynamics at a Flexible Glycosidic Linkage Revealed by NMR Spectroscopy and Molecular Dynamics Simulations: Analysis of β-L-Fucp-(1→6)-α-D-Glcp-OMe in Water Solution, *J. Phys. Chem. B*, 2013, **117**, 14709–14722.

18 M. J. Thrippleton and J. Keeler, Elimination of zero-quantum interference in two-dimensional NMR spectra, *Angew. Chem., Int. Ed.*, 2003, **42**, 3938–3941.

19 A. M. Dixon, G. Widmalm and T. E. Bull, Modified GOESY in the analysis of disaccharide conformation, *J. Magn. Reson.*, 2000, **147**, 266–272.

20 A. Meissner and O. W. Sørensen, Measurement of J(H,H) and long-range J(X,H) coupling constants in small molecules. Broadband XLOC and J-HMBC, *Magn. Reson. Chem.*, 2001, **39**, 49–52.

21 T. Nishida, G. Widmalm and P. Sandor, Hadamard long-range proton-carbon coupling constant measurements with band-selective proton decoupling, *Magn. Reson. Chem.*, 1995, **33**, 596–599.

22 T. Nishida, G. Widmalm and P. Sandor, Hadamard Long-Range Proton—Carbon Coupling Constant Measurements with Pulsed Field Gradients, *Magn. Reson. Chem.*, 1996, **34**, 377–382.

23 F. del Río-Portilla, V. Blechta and R. Freeman, Measurement of Poorly Resolved Splittings by J Doubling in the Frequency Domain, *J. Magn. Reson., Ser. A*, 1994, **111**, 132–135.

24 E. Säwén, T. Massad, C. Landersjö, P. Damberg and G. Widmalm, Population distribution of flexible molecules from maximum entropy analysis using different priors as

6992 | *Org. Biomol. Chem.*, 2023, **21**, 6979–6994

This journal is © The Royal Society of Chemistry 2023

background information: application to the φ,ψ-conformational space of the α-(1→2)-linked mannose disaccharide present in N- and O-linked glycoprotein, *Org. Biomol. Chem.*, 2010, **8**, 3684–3695.

25 O. Guvench, E. R. Hatcher, R. M. Venable, R. W. Pastor and A. D. MacKerell, Jr., CHARMM Additive All-Atom Force Field for Glycosidic Linkages between Hexopyranoses, *J. Chem. Theory Comput.*, 2009, **5**, 2353–2370.

26 O. Guvench, S. N. Greene, G. Kamath, J. W. Brady, R. M. Venable, R. W. Pastor and A. D. MacKerell, Jr., Additive Empirical Force Field for Hexopyranose Monosaccharides, *J. Comput. Chem.*, 2008, **29**, 2543–2564.

27 M. J. Abraham, T. Murtola, R. Schulz, S. Páll, J. C. Smith, B. Hess and E. Lindahl, GROMACS: High performance molecular simulations through multi-level parallelism from laptops to supercomputers, *SoftwareX*, 2015, **1–2**, 19–25.

28 J. Lee, X. Cheng, J. M. Swails, M. S. Yeom, P. K. Eastman, J. A. Lemkul, S. Wei, J. Buckner, J. C. Jeong, Y. Qi, S. Jo, V. S. Pande, D. A. Case, C. L. Brooks, A. D. MacKerell, Jr., J. B. Klauda and W. Im, CHARMM-GUI Input Generator for NAMD, GROMACS, AMBER, OpenMM, and CHARMM/OpenMM Simulations Using the CHARMM36 Additive Force Field, *J. Chem. Theory Comput.*, 2016, **12**, 405–413.

29 G. Bussi, D. Donadio and M. Parrinello, Canonical sampling through velocity rescaling, *J. Chem. Phys.*, 2007, **126**, 014101.

30 M. Parrinello and A. Rahman, Polymorphic transitions in single crystals: A new molecular dynamics method, *J. Appl. Phys.*, 1981, **52**, 7182–7190.

31 R. W. Hockney, The potential calculation and some applications, *Methods Comput. Phys.*, 1970, **9**, 135–211.

32 W. L. Jorgensen, J. Chandrasekhar, J. D. Madura, R. W. Impey and M. L. Klein, Comparison of simple potential functions for simulating liquid water, *J. Chem. Phys.*, 1983, **79**, 926–935.

33 S. Miyamoto and P. A. Kollman, SETTLE: An analytical version of the SHAKE and RATTLE algorithm for rigid water models, *J. Comput. Chem.*, 1992, **13**, 952–962.

34 B. Hess, P-LINCS: A parallel linear constraint solver for molecular simulation, *J. Chem. Theory Comput.*, 2008, **4**, 116–122.

35 T. Darden, D. York and L. Pedersen, Particle mesh Ewald: An N log(N) method for Ewald sums in large systems, *J. Chem. Phys.*, 1993, **98**, 10089–10092.

36 G. Bussi, F. L. Gervasio, A. Laio and M. Parrinello, Free-Energy Landscape for β Hairpin Folding from Combined Parallel Tempering and Metadynamics, *J. Am. Chem. Soc.*, 2006, **128**, 13435–13441.

37 Y. Sugita and Y. Okamoto, Replica-exchange molecular dynamics method for protein folding, *Chem. Phys. Lett.*, 1999, **314**, 141–151.

38 A. Barducci, G. Bussi and M. Parrinello, Well-tempered metadynamics: A smoothly converging and tunable free-energy method, *Phys. Rev. Lett.*, 2008, **100**, 020603.

39 G. A. Tribello, M. Bonomi, D. Branduardi, C. Camilloni and G. Bussi, PLUMED 2: New feathers for an old bird, *Comput. Phys. Commun.*, 2014, **185**, 604–613.

40 F. Neese, F. Wennmohs, U. Becker and C. Riplinger, The ORCA quantum chemistry program package, *J. Chem. Phys.*, 2020, **152**, 224108.

41 A. D. Becke, Density-functional exchange-energy approximation with correct asymptotic behavior, *Phys. Rev. A*, 1988, **38**, 3098–3100.

42 A. Schäfer, C. Huber and R. Ahlrichs, Fully optimized contracted Gaussian basis sets of triple zeta valence quality for atoms Li to Kr, *J. Chem. Phys.*, 1994, **100**, 5829–5835.

43 M. J. Field, P. A. Bash and M. Karplus, A combined quantum mechanical and molecular mechanical potential for molecular dynamics simulations, *J. Comput. Chem.*, 1990, **11**, 700–733.

44 K. Gaweda and W. Plazinski, Pyranose ring conformations in mono- and oligosaccharides: A combined MD and DFT approach, *Phys. Chem. Chem. Phys.*, 2017, **19**, 20760–20772.

45 W. Plazinski, M. U. Roslund, E. Säwén, O. Engström, P. Tähtinen and G. Widmalm, Tautomers of N-acetyl-D-allosamine: an NMR and computational chemistry study, *Org. Biomol. Chem.*, 2021, **19**, 7190–7201.

46 M. W. Lodewyk, M. R. Siebert and D. J. Tantillo, Computational Prediction of 1H and 13C Chemical Shifts: A Useful Tool for Natural Product, Mechanistic, and Synthetic Organic Chemistry, *Chem. Rev.*, 2012, **112**, 1839–1862.

47 M. J. Frisch, G. W. Trucks, H. B. Schlegel, G. E. Scuseria, M. A. Robb, J. R. Cheeseman, G. Scalmani, V. Barone, B. Mennucci, G. A. Petersson, H. Nakatsuji, M. Caricato, X. Li, H. P. Hratchian, A. F. Izmaylov, J. Bloino, G. Zheng, J. L. Sonnenberg, M. Hada, M. Ehara, K. Toyota, R. Fukuda, J. Hasegawa, M. Ishida, T. Nakajima, Y. Honda, O. Kitao, H. Nakai, T. Vreven, J. A. Montgomery Jr., J. E. Peralta, F. Ogliaro, M. Bearpark, J. J. Heyd, E. Brothers, K. N. Kudin, V. N. Staroverov, R. Kobayashi, J. Normand, K. Raghavachari, A. Rendell, J. C. Burant, S. S. Iyengar, J. Tomasi, M. Cossi, N. Rega, J. M. Millam, M. Klene, J. E. Knox, J. B. Cross, V. Bakken, C. Adamo, J. Jaramillo, R. Gomperts, R. E. Stratmann, O. Yazyev, A. J. Austin, R. Cammi, C. Pomelli, J. W. Ochterski, R. L. Martin, K. Morokuma, V. G. Zakrzewski, G. A. Voth, P. Salvador, J. J. Dannenberg, S. Dapprich, A. D. Daniels, Ö. Farkas, J. B. Foresman, J. V. Ortiz, J. Cioslowski and D. J. Fox, *Gaussian 09, Revision E.01*, Gaussian, Inc., Wallingford CT, 2009.

48 A. D. Becke, Density-functional thermochemistry. III. The role of exact exchange, *J. Chem. Phys.*, 1993, **98**, 5648–5652.

49 W. J. Hehre, L. Radom, P. von R. Schleyer and J. Pople, *AB INITIO Molecular Orbital Theory*, Wiley-Interscience, 1986.

50 M. Cossi, V. Barone, R. Cammi and J. Tomasi, Ab initio study of solvated molecules: a new implementation of the polarizable continuum model, *Chem. Phys. Lett.*, 1996, **255**, 327–335.

51 K. Wolinski, J. F. Hinton and P. Pulay, Efficient implementation of the gauge-independent atomic orbital method for NMR chemical shift calculations, *J. Am. Chem. Soc.*, 1990, **112**, 8251–8260.

This journal is © The Royal Society of Chemistry 2023

Org. Biomol. Chem., 2023, **21**, 6979–6994 | **6993**

52 W. Deng, J. R. Cheeseman and M. J. Frisch, Calculation of Nuclear Spin - Spin Coupling Constants of Molecules with First and Second Row Atoms in Study of Basis Set Dependence, *J. Chem. Theory Comput.*, 2006, **2**, 1028–1037.

53 P.-E. Jansson, L. Kenne and G. Widmalm, CASPER-a computerised approach to structure determination of polysaccharides using information from n.m.r. spectroscopy and simple chemical analyses, *Carbohydr. Res.*, 1987, **168**, 67–77.

54 M. V. Zaccheus, R. Pendrill, T. A. Jackson, A. Wang, F.-I. Auzanneau and G. Widmalm, Conformational Dynamics of a Central Trisaccharide Fragment of the LeaLex Tumor Associated Antigen Studied by NMR Spectroscopy and Molecular Dynamics Simulations, *Eur. J. Org. Chem.*, 2012, 4705–4715.

55 C. Landersjö, R. Stenutz and G. Widmalm, Conformational flexibility of carbohydrates: A folded conformer at the ϕ dihedral angle of a glycosidic linkage, *J. Am. Chem. Soc.*, 1997, **119**, 8695–8698.

56 J. Dabrowski, H. Grosskurth, T. Kožár and N. E. Nifant'ev, Conformational Mobility of Oligosaccharides: Experimental Evidence for the Existence of an "Anti" Conformer of the Galβl-3Glcβ1-OMe Disaccharide, *J. Am. Chem. Soc.*, 1995, **117**, 5534–5539.

57 C. Höög, C. Landersjö and G. Widmalm, Oligosaccharides display both rigidity and high flexibility in water as determined by ^{13}C NMR relaxation and 1H,1H NOE spectroscopy: evidence of anti-ϕ and anti-ψ torsions in the same glycosidic linkage, *Chem. – Eur. J.*, 2001, **7**, 3069–3077.

58 P. Vidal, J. Jiménez-Barbero and J. F. Espinosa, Conformational flexibility around the Gal-β-(1→3)-Glc linkage: Experimental evidence for the existence of the anti-ψ conformation in aqueous solution, *Carbohydr. Res.*, 2016, **433**, 36–40.

59 J. Kapla, O. Engström, B. Stevensson, J. Wohlert, G. Widmalm and A. Maliniak, Molecular dynamics simulations and NMR spectroscopy studies of trehalose-lipid bilayer systems, *Phys. Chem. Chem. Phys.*, 2015, **17**, 22438–22447.

60 A. Ruda, G. Widmalm and J. Wohlert, O-methylation in carbohydrates: An NMR and MD simulation study with application to methylcellulose, *J. Phys. Chem. B*, 2021, **125**, 11967–11979.

61 I. Ivarsson, C. Sandström, A. Sandström and L. Kenne, ^{1}H NMR chemical shifts of hydroxy protons in conformational analysis of disaccharides in aqueous solution, *J. Chem. Soc., Perkin Trans. 2*, 2000, 2147–2152.

62 S. Bekiroglu, L. Kenne and C. Sandström, NMR study on the hydroxy protons of the Lewis X and Lewis Y oligosaccharides, *Carbohydr. Res.*, 2004, **339**, 2465–2468.

63 C. Höög and G. Widmalm, Molecular dynamics simulation and nuclear magnetic resonance studies of the terminal glucotriose unit found in the oligosaccharide of glycoprotein precursors, *Arch. Biochem. Biophys.*, 2000, **377**, 163–170.

64 M. Iannuzzi, A. Laio and M. Parrinello, Efficient Exploration of Reactive Potential Energy Surfaces Using Car-Parrinello Molecular Dynamics, *Phys. Rev. Lett.*, 2003, **90**, 238302.

65 M. Yang, T. Angles d'Ortoli, E. Säwén, M. Jana, G. Widmalm and A. D. MacKerell, Jr., Delineating the conformational flexibility of trisaccharides from NMR spectroscopy experiments and computer simulations, *Phys. Chem. Chem. Phys.*, 2016, **18**, 18776–18794.

6994 | *Org. Biomol. Chem.*, 2023, **21**, 6979–6994

This journal is © The Royal Society of Chemistry 2023